

Heating of Intergalactic Gas and Cluster Scaling Relations

Michael Loewenstein¹

Laboratory for High Energy Astrophysics, NASA/GSFC, Code 662, Greenbelt, MD 20771

ABSTRACT

X-ray observations of galaxy groups and clusters are inconsistent with the predictions of the simplest hierarchical clustering models, wherein non-baryonic and baryonic components are assembled together under the sole influence of gravity. These departures are in the sense that the intergalactic medium is hotter and more extended than expected, and become increasingly strong for less massive systems. I model these effects by constructing baseline sequences of hydrostatic polytropic models normalized to observations of high-temperature clusters and numerical simulations, and then transforming them by adding proscribed amounts of heat per particle at the cluster center. I present sequences with a universal value of this heating parameter that simultaneously reproduce recently published observed (gas and total gravitational) mass-temperature and entropy-temperature relations. The required amount of energy injection is consistent with constraints on the number of supernovae needed to account for observed intracluster silicon abundances, provided that energy injection is centrally concentrated. I argue that most of the heating occurred during or after the assembly of the cluster, and not exclusively in pre-collapse proto-cluster fragments.

Subject headings: galaxies: clusters: general — intergalactic medium — cosmology

1. Context

Hierarchical clustering in a universe where non-baryonic dominates over baryonic matter is the primary heuristic framework for studying large scale structure formation; and, one of the primary laboratories for disconfirming variations deriving from particular combinations

¹Also with the University of Maryland Department of Astronomy

of fluctuation spectrum and cosmological world model is the ensemble of clusters of galaxies.² Such distinguishing characteristics of the cluster population include the two-point correlation function and mass function of collapsed non-baryonic halos (e.g., Governato et al. 1999).

Since non-baryonic matter is not amenable to observation, these relationships must be studied indirectly through gravitational lensing and baryonic tracers such as stars (in galaxies) and hot intergalactic gas. The latter, perhaps the most unambiguous tracer because of the density-squared dependence of the hot gas emissivity, is the focus of the present study. The now well-developed database of cluster X-ray observations made throughout this decade by the *ROSAT* and *ASCA* observatories have provided accurate measurements of the cluster temperature function (e.g., Markevitch 1998), and $\log N - \log S$ relation (e.g., Jones et al. 1998); however, mapping from these to the relevant non-baryonic halo relations requires knowledge of the thermal and dynamical structure and history of the intracluster medium (ICM).

In the most well-studied hierarchical clustering scenarios, structure formation is merger-driven, proceeding sequentially from small to large scales. A remarkable result of numerical simulations along these lines is that the mass density profiles of relaxed, non-baryonic halos can be characterized by a universal functional form (Navarro, Frenk, & White 1997 – hereafter NFW; Jing 1999) – at least over some large radial range. These halos are not precisely self-similar, since less massive halos tend to collapse earlier when the universe was more dense and thus have – on average – more concentrated non-baryonic density distributions. Subject to collisional processes such as shocks, the structure of the baryonic component will differ from that of the non-baryonic, but in a regular and predictable manner if the two components simply approach equilibrium in concert (e.g., Eke, Navarro, & Frenk 1998).

However, there is ample observational evidence for departures from such simplicity – evidence that becomes more striking as one focuses on less massive systems. The most well-established such breakdown is the relative steepness of the correlation between X-ray luminosity and ICM temperature (T_x), with $L_x \propto T_x^{\sim 3}$ observed in contrast to $L_x \propto T_x^{\sim 2}$ predicted if gravitational collapse is the sole mechanism driving the evolution of both components (e.g., Arnaud & Evrard 1999). Likewise, values of T_x very near the non-baryonic component virial temperature are predicted, an equality that evidently increasingly breaks down for less massive systems based on departures from $\mu m_p \sigma^2 = kT_x$ (e.g., Bird, Mushotzky, & Metzler 1995) and $M \propto T_x^{3/2}$ (Horner, Mushotzky, & Scharf 1999; Ettori & Fabian 1999

²For simplicity – and because there is no universally accepted demarcation – I follow Jones et al. (1998) in referring to all bound collections of galaxies as clusters, therein subsuming the usual definition of groups of galaxies.

– hereafter EF), where μm_p is the mean mass per particle, σ the one-dimensional cluster velocity dispersion, and M the total mass (evaluated at r_{500} : the radius within which the average density contrast, relative to the critical density, is 500). There is also evidence for a concomitant increase in ICM extent from the steepness of the $M_{ICM}-T_x$ correlation (where M_{ICM} is the ICM gas mass within r_{500} ; Mohr, Mathiesen, & Evrard 1999), and the gradual flattening towards low temperatures of the relation between entropy and T_x (the “entropy floor;” Ponman, Cannon, & Navarro 1999 – hereafter PCN).

All of these deviations from predictions where ICM structure is exclusively determined by gravitational collapse are indicative of an important role for extra-gravitational heating in determining ICM properties and their variation with mass. Understanding the magnitude and source of the heating not only is necessary for mapping from observed X-ray properties to those of the non-baryonic component, but also sheds light on galaxy formation since feedback from the earliest star formation epoch is the most likely heating mechanism. Since most metals in the universe are produced in objects of high overdensity (Cen & Ostriker 1999), and are subsequently ejected into intergalactic space by supernova-driven galactic outflows (Pettini 1999), measurements of ICM heavy metal enrichment provide independent constraints on the magnitude of energy injection (White 1991, Loewenstein & Mushotzky 1996).

I address this set of interconnected puzzles in the present work as follows. Adopting the most widely-used functional form for the non-baryonic density distribution that is completely determined by a single concentration parameter, baseline mass sequences of equilibrium, polytropic ICM configurations are constructed. The sequences are anchored at the high mass end using the results of high-temperature ICM observations and simulations (that are mutually consistent), and then extended to lower masses following specified mass-scalings of the non-baryonic halo concentration. A thermodynamic perspective proves physically illuminating (Bower 1997; Balogh, Babul, & Patton 1999), and so heated families of mass sequences are calculated that differ from the baseline sequences by fixed amounts of heating at the cluster center. It then remains to be seen whether the mass sequence in a particular family can simultaneously explain all of the observed deviations from the scaling relations predicted by models without heating, while also conforming with the nucleosynthetic constraints from ICM abundance studies. I will show that, in fact, they do so.

2. The Baseline Configuration

In this section I construct simple analytic models that accurately reproduce the observed and simulated ICM distribution of the most massive clusters. This serves as a useful point

of departure for creating heated distributions for the entire range of cluster masses.

2.1. Polytropic Models

I consider spherically symmetric, hydrostatic gas configurations in a total gravitational potential following the NFW prescription. Thus,

$$\frac{1}{\rho_{\text{gas}}} \frac{dP_{\text{gas}}}{dr} = -\frac{GM_{\text{grav}}(< r)}{r^2}, \quad (1)$$

where ρ_{gas} and P_{gas} are the ICM density and pressure distributions, respectively. M_{grav} is the total gravitational mass given by

$$M_{\text{grav}}(< r) = M_{\text{virial}} \frac{F_{\text{NFW}}(r/a_{\text{NFW}})}{F_{\text{NFW}}(c)}, \quad (2)$$

where

$$F_{\text{NFW}}(x) \equiv \ln(1+x) - \frac{x}{1+x}; \quad (3)$$

a_{NFW} is the non-baryonic mass distribution scale-length, c the concentration parameter $r_{\text{virial}}/a_{\text{NFW}}$, and r_{virial} the virial radius. Models that are analytic and conveniently flexible are obtained under the polytropic assumption, $P_{\text{gas}} \propto \rho_{\text{gas}}^{1+1/n}$ (Suto, Sasaki, & Makino 1998; Cavaliere, Menci, & Tozzi 1999; EF). The polytropic gas distribution is determined by the single function

$$\theta(x) \equiv 1 + A \left[\frac{\ln(1+x)}{x} - 1 \right]. \quad (4)$$

The gas temperature and density follow from $T_{\text{gas}} = T_o \theta(r/a_{\text{NFW}})$ and $\rho_{\text{gas}} = \rho_o \theta^n(r/a_{\text{NFW}})$, respectively, where T_o and ρ_o are the (assumed finite) central values of gas temperature and density. The constant

$$A \equiv \frac{2c}{F_{\text{NFW}}(c)} \frac{T_{\text{virial}}}{(n+1)T_o} \quad (5)$$

must not exceed a maximum value to assure non-negative temperature and density out to r_{virial} , *i.e.* there is a minimum ratio of T_o/T_{virial} for each pair (c, n) . In the isothermal limit ($n \rightarrow \infty$), the density distribution is given instead by

$$\rho_{\text{gas}} = \rho_{\infty} \theta_{\text{iso}}(r/a_{\text{NFW}}), \quad (6)$$

where

$$\theta_{\text{iso}}(x) = (1+x)^{A_{\text{iso}}/x}, \quad (7)$$

and

$$A_{\text{iso}} \equiv \frac{2c}{F_{\text{NFW}}(c)} \frac{T_{\text{virial}}}{T_{\text{gas}}} \quad (8)$$

(Makino, Sasaki, & Suto 1998; EF). The gas density at the origin for the isothermal case is related to that at infinity by $\rho_o = \rho_\infty e^{A_{\text{iso}}}$.

The virial mass, radius, and temperature are connected through the relationships

$$M_{\text{virial}} = \frac{4\pi}{3} r_{\text{virial}}^3 \Delta_c \rho_{\text{crit}} \quad (9)$$

and

$$\frac{kT_{\text{virial}}}{\mu m_p} = \frac{1}{2} \frac{GM_{\text{virial}}}{r_{\text{virial}}}, \quad (10)$$

where Δ_c is the density contrast (with respect to the critical density $\rho_{\text{crit}} = 9.21 \cdot 10^{-30} h_{70}^2 \text{ g cm}^{-3}$; h_{70} is the Hubble constant in units of $70 \text{ km s}^{-1} \text{ Mpc}^{-1}$) within which virial equilibrium is established.

In addition to the concentration parameter, c , and polytropic index, n , I parameterize models by quantities more observationally relevant than T_o and ρ_o – the global gas fraction, $f_{\text{virial}} \equiv f_{\text{gas}}(r_{\text{virial}})$, and density-squared-weighted average temperature in virial units, τ . It follows that

$$\frac{T_o}{T_{\text{virial}}} = \tau \frac{I_{2n}(c)}{I_{2n+1}(c)}, \quad (11)$$

and

$$\frac{\rho_o}{\rho_{\text{crit}}} = \frac{\Delta_c}{3} c^3 f_{\text{virial}} I_n(c)^{-1}, \quad (12)$$

where

$$I_m(c) \equiv \int_0^c dx x^2 \theta(x)^m. \quad (13)$$

Equation (11) must be solved iteratively.

2.2. The Baseline Model

In order to establish a baseline sequence of models without extra-gravitational heating, I first turn to the literature on numerical simulations. In particular, I consider the average $z = 0$ model in an $\Omega_o = 0.3$, $\Lambda_o = 0.7$, $h_{70} = 1$ cosmology from Eke et al. (1998). Although the demographic properties of the cluster population greatly depend on world model, the $z = 0$ structure of the most massive clusters is relatively insensitive to this choice. The non-baryonic component in the simulated cluster is completely characterized by $M_{\text{virial}} =$

$1.51 \cdot 10^{15} h_{70}^{-1} M_{\odot}$, $\Delta_c = 100$ ($r_{\text{virial}} = 2.99 h_{70}^{-1}$ Mpc, $kT_{\text{virial}} = 6.9$ keV), and $c = 6.47$; the gas component by $f_{\text{virial}} = 0.087$ (by assumption), $T_x \approx T_{\text{virial}}$ ($\tau = 1$), and

$$\rho_{\text{gas}} \approx \rho_{\text{crit}} \delta_o \left(1 + \frac{r^2}{r_{\text{core}}^2} \right)^{-3\beta_{\text{fit}}/2}, \quad (14)$$

with $\delta_o = 1970$, $r_{\text{core}}/r_{\text{virial}} \approx 0.05$, and $\beta_{\text{fit}} = 0.735$.

Temperature profiles measured with *ASCA* have been characterized by $n \approx 5$ polytropic distributions (Markevitch et al. 1998); however, both temperature (Irwin, Bregman, & Evrard 1999) and density profiles in hydrostatic models with this index are significantly steeper than those in the simulations. In fact, the density distribution in the ICM of the simulated cluster is accurately recovered only in models approaching the isothermal limit. Moreover, the best fit has $\tau = 1.1$ rather than $\tau = 1$. Figure 1 shows a comparison between the simulated cluster density profile expressed by equation (14) and models with $f_{\text{virial}} = 0.087$ and $(n, \tau) = (5, 1.1)$, $(100, 1)$, and $(100, 1.1)$ – clearly the last provides the superior fit. The cause of the deviation of the temperature profile in the numerical simulation, with its mild gradient at large radii, from its characterization in the baseline model is evidently due to residual unthermalized bulk kinetic energy in the simulated ICM at $r > 0.5r_{\text{virial}}$. This has little effect on the observed cluster-wide temperature – generally, an emission-weighted average over $\sim 0.5r_{\text{virial}}$ – that is the the global temperature used in the correlations considered in this paper.

In a recent paper, EF describe the results of their analysis of *ROSAT* PSPC data on the ICM in 36 high-temperature clusters. The mean parameters that emerge from surface brightness fitting, using functions of the forms expressed in both equations (6) and (14), display a remarkable agreement with the above. They find mean values of β_{fit} and $a_{\text{NFW}}/r_{\text{core}}$ of 0.72 and 3.17 compared to 0.735 and 3.08 in the simulations of Eke et al. (1998). However, while (on average) $A_{\text{iso}} = 11.3$ in the latter, EF find $A_{\text{iso}} = 10.3$ from fitting the surface brightness profile using equation (6) – corresponding to $\tau = 1.1$ as expected (Figure 1). The mass-temperature relationship derived by EF is also consistent with $\tau = 1.1$ at the high- T_x end.

The appropriate value of the global gas fraction, f_{virial} , can be estimated from the values of M_{ICM} at the highest T_x (where effects of heating should be minimized) calculated within r_{500} by Mohr et al. (1999).³ Extrapolating to r_{virial} using an $n = 100$ polytrope with $\tau = 1.1$

³ICM masses derived in EF (1999) generally agree with those in Mohr et al. (1999) for clusters in common to the two papers, although there are significant discrepancies in gas mass fraction due to differences in adopted temperatures and mass estimation technique.

in an NFW potential with $r_{\text{virial}}/a_{\text{NFW}} = 6.2$ corresponding to $kT_x = 10$ keV ($M_{\text{virial}} = 2.3 \cdot 10^{15} h_{70}^{-1} M_{\odot}$) yields $f_{\text{virial}} = 0.155 h_{70}^{-3/2}$ (extrapolated from $f_{\text{gas}} = 0.136 h_{70}^{-3/2}$ at r_{500}).

To summarize, I adopt as baseline configurations hydrostatic models with a polytropic index of $n = 100$ normalized such that the emission-measure-weighted average temperature is $1.1 \times$ the virial temperature, and gas fraction within the virial radius $f_{\text{virial}} = 0.155 h_{70}^{-3/2}$ ($\rho_o = 5050 h_{70}^{-3/2} \rho_{\text{crit}}$). The gravitating mass is assumed to follow equations (2) and (3), with

$$c = c_{10} \left(\frac{M_{\text{virial}}}{M_{10}} \right)^{-\gamma}, \quad (15)$$

where $M_{10} = 2.3 \cdot 10^{15} h_{70}^{-1} M_{\odot}$ corresponds to the virial mass at a density contrast of 100 for a $kT_x = 10$ keV cluster, and $c_{10} = 6.2$ is adopted from Eke et al. (1998) assuming $\gamma = 0.1$ (appropriate for a CDM-like fluctuation spectrum; NFW). These models yield extremely accurate representations of the density distributions of observed average high-temperature clusters (as well as of numerical simulations of the same), and do so for the correct observed mean temperature. Any proposed heating mechanism must therefore have relatively little effect on the ICM of the most massive clusters.

The adopted models are virtually isothermal. Models where the inverse of the polytropic index is substantially different than zero (or where the temperature distribution is otherwise strongly varying with radius) have density distributions that are too steep to be consistent with the observations (as well as the simulations) if the ICM is in hydrostatic equilibrium in an NFW potential (this remains true for other concentration parameters than those considered above). Thus, if the temperature profiles reported in Markevitch et al. (1998) (recently brought into question by Irwin et al. 1999 and Kikuchi et al. 1999) hold up, either hydrostatic equilibrium, electron-ion equipartition (Ettori & Fabian 1997; Takizawa 1998), or the assumption of a NFW-type total mass profile must break down well within the virial radius.

3. Heated Families of Polytropic Mass Sequences

I now describe a simple prescription for constructing families of mass sequences for polytropic intracluster media in hydrostatic equilibrium in an NFW potential that deviate from the baseline sequence described above by having been heated by differing amounts. Heated families are completely determined by specifying the final gas fraction and polytropic index for each cluster mass. I show, for several different families, that a mass sequence corresponding to the heating needed to explain the observed entropy floor also reproduces

the other departures from gravity-only self-similarity described in Section 1.

3.1. Formalism

Consider a transformation from the baseline polytropic configuration to a new one:

$$\{n^{bl}, T_o^{bl}, \rho_o^{bl}\} \longrightarrow \{n, T_o, \rho_o\}, \quad (16)$$

where the bl superscript refers to the baseline model parameters. The changes in specific entropy and heat corresponding to the transformation are

$$\Delta s = \int ds = \frac{3}{2} \frac{k}{\mu m_p} \left[\ln \frac{T_o}{T_o^{bl}} - \frac{2}{3} \ln \frac{\rho_o}{\rho_o^{bl}} \right], \quad (17)$$

and

$$\Delta q = \int T ds = \frac{3}{2} \frac{k}{\mu m_p} (T_o - T_o^{bl}) \left[1 - \frac{2}{3} \frac{1}{T_o - T_o^{bl}} \int \frac{d \ln \rho}{d \ln T} dT \right], \quad (18)$$

where $ds = (3k/2\mu m_p) d \ln(T/\rho^{2/3})$ and the integrals extend from the baseline to the new configuration. One can define an effective adiabatic index, Γ , such that

$$\frac{T_o}{T_o^{bl}} = \left(\frac{\rho_o}{\rho_o^{bl}} \right)^{\Gamma-1}, \quad (19)$$

from which it follows that

$$\Delta s = C_\Gamma^{-1} \frac{k}{\mu m_p} \ln \frac{T_o}{T_o^{bl}} \quad (20)$$

and

$$\Delta q = C_\Gamma^{-1} D_\Gamma \frac{k}{\mu m_p} (T_o - T_o^{bl}) = D_\Gamma \frac{T_o - T_o^{bl}}{\ln(T_o/T_o^{bl})} \Delta s, \quad (21)$$

where

$$C_\Gamma \equiv \frac{2\Gamma - 2}{3\Gamma - 5}, \quad (22)$$

and

$$D_\Gamma = 1 + C_\Gamma (\Gamma - 1)^{-1} \left(1 - \frac{\Gamma - 1}{T_o - T_o^{bl}} \int \frac{d \ln \rho}{d \ln T} dT \right). \quad (23)$$

For a constant heating adiabat

$$\frac{d \ln \rho}{d \ln T} = \frac{1}{\Gamma - 1}; D_\Gamma = 1; \quad (24)$$

and, therefore

$$T_o = T_o^{bl} + C_\Gamma T_q; \rho_o = \rho_o^{bl} \left(1 + C_\Gamma \frac{T_q}{T_o^{bl}}\right)^{\frac{1}{\Gamma-1}}, \quad (25)$$

where T_q is defined such that, at the center, the new configuration has an extra heat per particle, $\Delta q = kT_q/\mu m_p$ relative to the baseline configuration. Non-decreasing entropy requires $\Gamma \leq 1$ (temperature increasing as density decreases) or $\Gamma \geq 5/3$ (temperature increasing as density increases). $\Gamma = 1$, $\Gamma = 0$, and $\Gamma = \infty$ correspond to isothermal, isobaric, and isochoric transformations, respectively; for $\Gamma = 1$ equation (25) is replaced by

$$T_o = T_o^{bl}; \rho_o = \rho_o^{bl} e^{-\frac{T_q}{T_o^{bl}}}. \quad (26)$$

I assume that the amount of heating per particle is the same for all clusters (and therefore less effective for more massive clusters), so that

$$\tau_q \equiv \frac{T_q}{T_{\text{virial}}} = \epsilon \left(\frac{M_{\text{virial}}}{M_{10}}\right)^{-\frac{2}{3}}, \quad (27)$$

where ϵ is the (assumed universal) injected heat per particle in units of 10 keV. To make a clearer connection with observationally relevant quantities, in place of T_q and Γ , ϵ and the slope ν are specified, assuming that the global gas fraction in the heated configuration is given by

$$f_{\text{virial}} = f_{10} \left(\frac{M_{\text{virial}}}{M_{10}}\right)^\nu, \quad (28)$$

where f_{10} is the global gas fraction for a cluster with a 10 keV ICM (f_{virial} is generally assumed constant with mass along baseline mass sequences).

The prescription for calculating heated families of polytropic mass sequences can be summarized as follows. (1) Baseline mass sequences are determined from specification of the concentration-mass relation (the parameter γ in equation 15), f_{10} ($0.155h_{70}^{-3/2}$), n^{bl} (100), and τ (1.1). (2) A heated family is then computed, having specified ν and n , by varying ϵ . In practice, for each mass (and its appropriate f_{virial} from equation 28 and concentration c from equation 15) hydrostatic models are iterated on the parameter $\Delta\tau \equiv (T_o - T_o^{bl})/T_{\text{virial}}$ until the desired value of ϵ is achieved. The relationship between ϵ and $\Delta\tau$ is approximated as

$$\epsilon = \frac{3}{2} \left(\frac{M_{\text{virial}}}{M_{10}}\right)^{\frac{2}{3}} \Delta\tau \left(1 - \frac{2}{3} \frac{\ln(\rho_o/\rho_o^{bl})}{\ln(1 + \Delta\tau/\tau)}\right), \quad (29)$$

which is exact if the heating is along an adiabat with a constant index Γ .

3.2. A Simple Heated Family

For simplicity, I initially consider a heated family where the gas fraction, f_{virial} , and polytropic index, n , are identical to those in the baseline model (*i.e.* $\nu = 0$ and $n = 100$; also $\gamma = 0.1$). Perhaps the most striking evidence for significant heating of the ICM in a form similar to that of equation (27) is the entropy floor at low T_x recently reported by PCN, where the “entropy” is defined as $kT_x n_e^{-2/3}$; n_e is the electron density in cm^{-3} evaluated at r_c (r_c is defined as one-tenth the radius within which the total density contrast is 200, as estimated from T_x using the baseline sequence of models), and kT_x is in keV. The value of ϵ that produces an entropy-temperature relation with the observed entropy floor at ≈ 100 keV cm^2 is 0.35.⁴ This (dashed) curve is shown in Figure 2 along with observed data points (assuming $h_{70} = 1$) from analysis of *ASCA* imaging data (Fukazawa 1997; Hwang et al. 1999). Also shown is the value from numerical simulations (filled triangle; Eke et al. 1998), and the (solid) curve for $\epsilon = 0$. Note that the latter is slightly steeper than linear due to the more concentrated non-baryonic mass distributions for cooler clusters.

Remarkably, this same simple heated mass sequence is in excellent agreement with all of the other observed trends alluded to in Section 1. Figure 3 show a plot of total mass evaluated at r_{500} versus T_x for $\epsilon = 0$ (solid curve) and $\epsilon = 0.35$ (dashed curve). While most of the heating in the $\epsilon = 0.35$ sequence goes into decreasing the gas concentration, rather than increasing the temperature, less massive clusters are predicted to become increasingly hotter than expected in the absence of heating. For this sequence, $\Gamma \approx 0.8$ and $C_\Gamma \approx 0.15$ (see equations 19 and 22), nearly independent of mass, so that all clusters have an increase in internal energy per particle of $C_\Gamma kT_q \approx 0.5$ keV. The resulting predicted mass-temperature relationship is

$$M(r_{500}) \approx 1.32 \cdot 10^{15} \left(\frac{kT_x - 0.5\text{keV}}{9.5\text{keV}} \right)^{3/2} Q(M) h_{70}^{-1} M_\odot. \quad (30)$$

$Q(M)$ is a form factor relating $M(r_{500})$ to M_{virial} and increases from 1 at $kT_x = 10$ keV to 1.12 at $kT_x = 1$ keV for $\gamma = 0.1$ in equation (15). Equation (30) is in excellent accord with estimates from X-ray observations compiled by Horner et al. (1999; data points in Figure 3) and the best-fit mass-temperature trend from EF (stars in Figure 3). A similar accordance is found for the temperature dependence of gas mass within r_{500} (Figure 4, where the stars represent the best-fit trend from Mohr et al. 1999). In a similar vein to Figure 3,

⁴This value is sufficiently large that it has a non-negligible effect on even the hotter clusters, and I have reduced the dimensionless average temperature τ in the baseline model from 1.1 to 1.05 to preserve the high level of agreement with the observed density profiles for high- T_x clusters.

Figure 5 shows the $\epsilon = 0$ and 0.35 model variations of $(kT_{\text{virial}}/\mu m_p)^{1/2}$ with T_x that can be characterized by

$$kT_{\text{virial}} \approx \frac{kT_x - 0.5\text{keV}}{1.05}, \quad (31)$$

compared to observed values of the velocity dispersion σ from Girardi et al. (1998; data points) and the best-fit σ - T_x correlation of Bird et al. (1995; stars). The agreement with the best-fit trend is excellent; although, a large observed scatter is evident, and I have not considered velocity dispersion anisotropies and gradients that are possible sources of discrepancy between kT_{virial} and $\mu m_p \sigma^2$.

To summarize, if one considers cluster non-baryonic matter and gas distributions as predicted by large scale structure numerical simulations, and then transforms the gas distribution by adding 3.5 keV per particle of heat at the center while preserving the global baryon fraction and polytropic index, the observed trends wherein the ICM becomes increasingly hotter and more extended⁵ are simultaneously and accurately reproduced.

3.3. Other Heated Families

With families of mass sequences anchored at high- T_x as described in Section 2.2, there remains the freedom to vary the following three (one for the gravitating mass, two for the ICM) slope parameters: the mass-scalings of total matter concentration – $\gamma \equiv -\text{d} \ln c / \text{d} \ln M_{\text{virial}}$ – and gas fraction within the virial radius – $\nu \equiv \text{d} \ln f_{\text{virial}} / \text{d} \ln M_{\text{virial}}$, and the polytropic index in the heated configuration – $n \equiv \text{d} \ln \rho_{\text{gas}} / \text{d} \ln T_{\text{gas}}$. The implications of varying these are as follows.

Since an increase in the concentration of the gravitating mass distribution increases the central ICM density in the equilibrium configuration, a steeper dependence of c on M_{virial} (as would be expected if the fluctuation spectrum is flatter than in CDM cosmogonies; NFW) would imply that more heating (larger ϵ) be required to explain the observed entropy floor. For example ~ 4.5 keV per particle would be required if γ were increased from 0.1 to 0.2 (that is the concentration increases by ~ 2.3 instead of ~ 1.5 for 1 keV, relative to 10 keV, clusters).

Positive values of the parameter ν correspond to cooler, less massive clusters having

⁵Mohr et al. (1999) claim an absence of evidence of a more extended ICM in cooler clusters because of the lack of a clear trend of the average gas particle location with temperature; however, the scenario described above predicts that this does not become noticeable until temperatures below those of the clusters in their sample.

progressively smaller baryon fractions within the virial radius. The heating required to produce the observed entropy floor can be reduced to ~ 2.5 keV per particle for $\nu = 0.25$ (implying a baryon fraction in 1 keV clusters nearly three times lower than in 10 keV clusters). It is implicitly assumed that the reduction in f_{virial} (by mass leaving the cluster, or simply expanding beyond r_{virial}) is a result of the heating: lower values of ϵ can be accommodated if, instead, cooler clusters are assumed to be intrinsically gas-poor. However, the magnitude of the entropy gap between observed cool clusters and that expected assuming no heating and constant f_{virial} would require an extreme gas-fraction trend (PCN) of which there is no observational evidence (EF, Mohr et al. 1999).

Finally, I have considered a family of mass sequences where the polytropic index in the heated model decreases by 50% for each factor of two decrease in mass (*i.e.* from $n = 100$ to $n \approx 11$ as T_x – defined as the emission-measure-averaged ICM temperature within r_{500} – varies from 10 to 1 keV), as might be appropriate if heating leads to more-nearly isentropic configurations (Balogh et al. 1999). Since as n decreases the ICM density distribution steepens, larger values of ϵ – corresponding to ~ 4.5 keV per particle – are demanded by the observed entropy floor.

One can conclude from the above that the observed entropy floor for cooler clusters is consistent with a mass sequence of polytropic equilibrium configurations heated by > 3 keV per particle at the cluster center (see Figure 2; 3 keV is about the temperature at which the observations start to deviate significantly from the predictions of models without heating). In the context of these models, this same amount of heat simultaneously accounts for the observed steepening of the relationship between ICM mass within r_{500} and temperature (Figure 4). Note that the former is a local indicator of ICM expansion, while the latter is a global indicator. Also note that any contrivance meant to lower the required amount of energy injection (e.g., by reducing the intrinsic gas fractions of cooler clusters), will destroy the simultaneous match to the observed steepening of the relationship between total mass within r_{500} and temperature (Figure 3) or, equivalently, the increasing departure from $T_x = T_{\text{virial}}$ implied by the observed σ - T_x relation (Figure 5).

4. Discussion

Given the striking success of the $\epsilon \sim 0.35$ heated family mass sequence in reproducing the observed trends in global ICM properties – in particular their monotonically increasing departure with decreasing temperature from expectations of models without extra-gravitational heating – it is worthwhile to consider the implications for the relative gas distributions in hot and cool clusters, the connection between heating and metal enrichment, and the astro-

physical interpretation of these models in the context of hierarchical formation of clusters.

4.1. Relative Gas Distributions

Clearly, the existence of an entropy floor caused by heating implies that cooler clusters will have more extended ICM, *i.e.* both lower central densities and shallower density slopes. And indeed this was discovered by PCN in their analysis of *ROSAT* cluster data. The effect of heating on the gas distribution is perhaps most evident in plots of the cumulative gas fraction. Figure 6 shows a comparison of these for 1 and 10 keV clusters with and without heating (the latter from the simple heated family of Section 3.2). In the absence of heating, cooler clusters are expected to have significantly higher gas fractions at small radii (relative to the virial radius) because of their more concentrated mass distributions. Including heating, the opposite is very strongly the case: at r_{500} ($\sim 0.5r_{\text{virial}}$), 1 keV clusters are about twice as gas-poor as 10 keV clusters (Figure 7), even though it is assumed that they have identical gas fractions at r_{virial} . A similarly strong trend is seen for the ICM density distribution slope, as shown by Figure 8 which plots $\beta_{\text{image}} \equiv 3\text{dln}\rho_{\text{gas}}/\text{dln}r$ at r_{500} versus T_x for mass sequences with and without heating. The density distribution is predicted to become flatter at all radii greater than $0.1r_{\text{virial}}$ for cooler clusters.

Whether these trends have been detected – and, if so, to what quantitative extent – is currently problematic. Since both the density slope and gas fraction vary (possibly non-monotonically) with radius, comparisons must be made at radii corresponding to identical density contrasts (e.g., r_{500}). Thus the total mass must be estimated (for cooler systems this must be done from the data itself, not from an extrapolation of the hot-cluster mass-temperature relation) in order to make a meaningful comparison of density slopes as well as gas fractions. Moreover, deriving the density distribution for the cooler clusters (*i.e.*, groups) is greatly complicated by uncertainties in background subtraction, in treating the emission from individual galaxies, and possibly by departures from spherical symmetry (Mulchaey & Zabludoff 1998, Hwang et al. 1999). Analysis along the lines of EF (who restrict themselves to the more luminous, and therefore hotter, systems) on the PCN ensemble of surface brightness profiles could prove illuminating. Interestingly, extended elliptical galaxy X-ray halos, with $kT_x \sim 0.7\text{-}1$ keV, tend to have $\beta_{\text{image}} \sim 0.5$, in accord with the heating sequence of Figure 8 and their likely physical continuity with ICM (Mathews & Brighenti 1998).

4.2. The Connection Between Heating and Metal Enrichment

The presently most reliable diagnostic of supernova heating in clusters – that presumably occurred during star formation driven galactic outflows at early epochs – is the ICM silicon abundance. Only iron abundances are determined more accurately; however, the amount of energy ejection associated with the mass of Fe in the ICM is sensitive to the poorly determined (e.g., Gibson, Loewenstein, & Mushotzky 1997) relative fractions of Fe originating from Type Ia (SNIa) and Type II (SNII) supernovae. Not only have accurate Si abundances been determined for a large sample of clusters (Fukazawa et al. 1999), but the explosion energy per Si yield is similar in standard SNIa and SNII models (e.g., Gibson et al. 1997) so that the energy injection associated with the observed amount of Si is robust to uncertainties in the SNIa/SNII ratio. The equivalent temperature of the injected energy can be expressed as

$$kT_q^{SN} \sim 1.6Z_{Si}e_{SN} \text{ keV}, \quad (32)$$

where Z_{Si} is the ICM Si abundance, relative to solar, and e_{SN} is the average injected energy per supernova (perhaps boosted by stellar winds from SNII progenitors; Leitherer & Heckman 1995) in units of 10^{51} erg.

Since Z_{Si} typically is ~ 0.7 for rich clusters (Fukazawa et al. 1999), supernova energy injection would seem to fall short by a factor of ~ 3 of providing the required heating (this problem is exacerbated for groups where the Si abundance is often estimated to be lower by an additional factor of two; Davis, Mulchaey, & Mushotzky 1999; Hwang et al. 1999). However, one must keep in mind that the requirement of 3 keV per particle of heating is for the cluster center only. If this heating were uniformly present cluster-wide, the resulting expansion of the ICM would lead to an extremely steep decrease of f_{virial} with mass. The fact that this is not observed implies that the energy injection decreases outward from the center. The central concentration of SN energy injection may be reflected in abundance gradients that have now been measured with *ASCA* (e.g., Ezawa et al. 1997). Additional heating at the cluster center could result from early AGN activity, although the mechanism for efficiently dissipating AGN energy flux in the ICM is unclear.

The average cluster-wide heating per particle can be estimated as $5C_{\Gamma}kT_q/2\mu m_p \sim 0.38kT_q/\mu m_p$, where C_{Γ} is defined in equation (22) and $\Gamma \approx 0.8$. Thus the global-average heating is on the order 1 keV per particle. This is more in line with that expected from nucleosynthetic considerations, but requires a high energy deposition efficiency into the ICM or $e_{SN} \gg 1$. The latter is possible if the initial mass function of SNII progenitors is skewed toward high masses (Timmes, Woosley, & Weaver 1996). This amount of energy injection exceeds the escape temperature of the lowest mass systems, and could lead to removal of some fraction of the ICM – depending on the detailed history of the heating with respect to

the dynamical evolution of the cluster. As discussed in the previous subsection, it is unclear whether lower mass systems have systematically lower gas fractions.

4.3. Physical Interpretation and the Epoch of Heating

The amount of heat characterizing the $\epsilon \sim 0.35$ heated family mass sequence corresponds to that required to transform the ICM from a non-heated equilibrium state, and is thus an upper limit since the gas may be pre-heated. If the heating occurs at sufficiently low density (*i.e.*, prior to cluster collapse), the energetic requirements for obtaining the observed entropy minimum are greatly reduced.

PCN argue that this must be the case. However, this is based in part on consideration of a SN rate (for the particular case of the Coma Cluster) derived from the present stellar content and the assumption of a standard initial mass function (IMF) that is well-established to fall far short of providing the observed heavy metal enrichment (e.g., Loewenstein & Mushotzky 1996). Using standard SN yields, the Si enrichment, in solar units, can be expressed as

$$Z_{Si} = 0.2 \left(\frac{10M_{\text{stars}}}{M_{\text{ICM}}} \right) \frac{\eta_{SN}}{0.01}, \quad (33)$$

where M_{stars} and M_{ICM} are the total cluster stellar and ICM masses, respectively, and η_{SN} is the total number of SN per solar mass of present-day stars. PCN, assuming $\eta_{SN} = 0.01$ as is appropriate for a standard IMF, thus derive an equivalent supernova temperature ~ 5 times lower than the value in equation (32) that is based on the actual observed rich cluster Si abundance. The relative epochs of cluster assembly and ICM heating cannot be constrained solely on energetic grounds.

In pre-heating models the ICM is heated to some initial temperature kT_* and high entropy state. The ICM in the lowest mass systems is spared any further entropy increase via accretion shocks but, instead, is accreted and compressed adiabatically – thus preserving the initial entropy at all radii. An entropy floor of the kind reported by PCN is predicted at low ICM temperature, and can be expressed as

$$n_e^{-2/3} kT = 100 \Sigma_o \text{ keV cm}^2 \quad (34)$$

with $\Sigma_o \sim 1$.

Consider two extreme variations on the pre-heating scenario. In the first (e.g., PCN), the universe as a whole is pre-heated to kT_* at a redshift of z_* and, therefore, an electron density of

$$n_{e*} = \Omega_{\text{baryon}} \frac{\rho_{\text{crit,o}}}{\mu_e m_p} (1 + z_*)^3 = 1.2 \cdot 10^{-7} (1 + z_*)^3 \text{ cm}^{-3} \quad (35)$$

(Tozzi & Norman 1999), where $\rho_{\text{crit},0}$ is the critical density at zero redshift, and $\Omega_{\text{baryon}} = 0.0255h_{70}^{-2}$ as implied by standard Big Bang nucleosynthesis. That is,

$$kT_* = 2.45 \cdot 10^{-3} \Sigma_o (1 + z_*)^2 \text{ keV}. \quad (36)$$

Reproducing the observed luminosity- and mass-temperature relations requires $kT_* \approx 0.5$ keV (Cavaliere et al. 1999), *i. e.* $z_* \approx 13$ for $\Sigma_o = 1$. In fact, however, to obtain the change in slope of the L_x - T_x relation (that is the transition to adiabatic compression) at the correct temperature requires $\Sigma_o = 2.5$ -10 (Tozzi & Norman 1999), implying $z_* = 3.5$ -8. That is, $\Sigma_o = 1$ can be reconciled with the mass-temperature relationship only if the universe was heated to 0.5 keV at a redshift greater than 10 – and, in this case, the transition from shock heating to adiabatic compression occurs at too low a mass to be consistent with the L_x - T_x relation. The transition occurs at the appropriate mass if the level of the entropy floor has been underestimated by a significant factor, however pre-heating redshifts greater than 3 are still required if the mass-temperature relation is to be recovered as well. Moreover, such a high initial entropy is predicted to lead to baryon fractions in groups only ~ 0.2 of the universal value (Cavaliere et al. 1999), which could be problematic since there are group baryon fractions observed to exceed 10% (Mulchaey et al. 1998, Hwang et al. 1999).

In the scenario of Balogh et al., each proto-cluster is heated at turnaround; *i.e.* they assume

$$n_{e*} = \Omega_{\text{baryon}} \frac{\rho_{\text{ta}}(z_*)}{\mu_e m_p} \approx 8.3 \cdot 10^{-6} g(z_*) (1 + z_*)^3 \text{ cm}^{-3} \quad (37)$$

for $\Omega_o = 0.3$ and $h_{70} = 1$, where $g(z_*) = 1, 0.88, 0.81,$ and 0.75 at $z_* = 1, 2, 3,$ and $5,$ respectively. Thus,

$$kT_* \approx 1.2 \cdot 10^{-2} g(z_*)^{2/3} \Sigma_o (1 + z_*)^2 \text{ keV}; \quad (38)$$

so that $kT_* = 0.5$ keV implies $z_* = 6.2$. The models of Balogh et al. (1999) also require $\Sigma_o > 1$ ($\Sigma_o \approx 3.7$) to explain the low-temperature steepening of the L_x - T_x relation.

Both pre-heating scenarios require an initial entropy several times greater than the observed entropy floor as estimated by PCN. These can perhaps be reconciled if one recalls that the PCN entropy floor is defined using a global average temperature. Pre-heating implies that accretion shocks become weak and the ICM increasingly isentropic at low temperature (well below where the entropy- and luminosity-temperature relations change slope, at $kT_x \sim 3$ keV). In the limit of pure adiabatic compression, significant temperature gradients are expected. As a result the local entropy at r_c may be larger than the PCN estimate.

One can consider pre-heated mass sequences of models as defined in Section 2, by fixing the polytropic index n at $3/2$. Such models are normalized by fixing two of the following three parameters: Σ_o , the mass-averaged temperature in units of the virial temperature

τ_m , and the gas fraction within the virial radius f_{virial} . A general feature of these models is that the ICM temperature at r_c is about 50% greater than the emission-averaged temperature, and the entropy at r_c correspondingly higher than that estimated using the emission-weighted average. Results for an isentropic mass sequence with $\Sigma_o = 2$ (chosen to approximately reproduce the PCN entropy floor) and $\tau_m = 1.05$ are shown by the dotted curves in Figures 3 and 4 (sequences with constant f_{virial} have similar properties at low T_x). The mass-temperature relation parallels that of the unheated sequence, shifted over by ~ 2 in temperature, so that the observed relation is well-matched at low T_x (Figure 3). The ICM mass-temperature relation is reproduced as well for $kT_x < 1.5$ keV (Figure 4), and only starts to deviate strongly beyond 2 keV (since the gas fraction exceeds 0.5) where the isentropic assumption should start to break down.

The temperature profile in the isentropic models are relatively steep (Figure 9). This can be compared to the observed gas distribution for HCG 62 – the best measured group temperature profile in terms of accuracy and extent. The density profile is flat as predicted, $n_e \sim r^{-1}$ (Ponman & Bertram 1993); but, for an isentropic distribution the temperature is expected fall to below 0.5 keV beyond 500 kpc – and does not (Finoguenov & Ponman 1999).

An assessment of the pre-heating scenario can now be summarized. If heating occurs prior to collapse, clusters with temperatures sufficiently below the turnover of the luminosity- (or, equivalently, the ICM mass-) and entropy-temperature relations are expected to be isentropic and display a steep trend of decreasing baryon fraction with decreasing temperature. The present observational evidence does not support this, although the existing data is not of sufficient quality to be conclusive. Moreover, to effect these turnovers at the appropriate mass scale requires an initial entropy at least twice the level of the observed entropy floor. In order to simultaneously explain the turnover in the mass-temperature relation the proto-cluster gas must be pre-heated to $kT_* > 0.3$ keV at redshift

$$z_* > 11\Sigma_o^{-1/2} \left(\frac{\mu_e m_p n_{e*}}{\Omega_{\text{baryon}} \rho_{\text{crit}}(z_*)} \right)^{1/3} - 1, \quad (39)$$

where the pre-collapse overdensity $(\mu_e m_p n_{e*})/(\Omega_{\text{baryon}} \rho_{\text{crit}}(z_*))$ must – by definition – lie between one and the overdensity at turnaround (~ 15). In the context of the thermal history of baryons in the universe (Cen & Ostriker 1999), such a level of pre-heating seems unlikely at that high a redshift. In fact the (mass-averaged) entropy in the baryon content of the universe is a strongly decreasing function of redshift, the universe having been both much cooler and more dense in the past, and does not approach the level of the observed cluster entropy floor until relatively recently.

Thus, I would conclude that pre-heating models in their present preliminary form cannot

simultaneously explain all of the heating-induced departures from self-similarity observed in clusters – although a definitive assessment must await more refined pre-heating models and their comparison with more extensive and complete observations of low-mass systems. On the other hand, the success of the heated families of equilibrium polytropes in simultaneously explaining the deviations from self-similarity observed in clusters (Figures 2-5) suggests that substantial heating – certainly in the cluster core – occurred after the cluster was, at least partially, in place. Perhaps some of the heating was triggered by merging activity associated with the latter stages of cluster formation. It must be noted, however, that the metal enrichment (or, at least, the Fe enrichment) that presumably accompanies the heating cannot have occurred much more recently than $z = 1$ based on the lack of evolution of cluster abundances (Mushotzky & Loewenstein 1997), and the properties of elliptical galaxies – the sites of primordial star formation generally presumed responsible for ICM heating and metal enrichment – as a function of redshift (Broadhurst & Bouwens 1999, and references therein).

A detailed consideration of these issues requires a fully time-dependent approach (e.g., Kay & Bower 1999), and must reconcile the required amount of heating with the observed properties of cluster galaxies (Wu et al., in preparation) – which may be problematic (Brighenti & Mathews 1999).

4.4. Cool Cluster Caveats

The breaking, by energy injection, of gravity-only self-similarity by an increasing amount for cooler clusters raises the following caveats. (1) In deriving the cluster mass function from X-ray luminosity (L_x) or temperature functions, care must be taken to avoid using single slope L_x - T_x or M - T_x relations extending all the way down from high T_x . (2) The gas fraction is a fairly steep function of radius for cool clusters (Figure 6) and values measured out to, e.g., r_{500} , may not accurately reflect the global value. Groups may appear gas-poor in comparison to rich clusters while, in fact, their ICM are simply more extended with respect to their non-baryonic components.

If hierarchical clustering correctly describes the formation of large scale structure, cooler clusters will tend to form over a wider range of redshifts (Balogh et al. 1999); and presumably, there will be greater variation in the relative timing of merging/collapse and star formation (*i.e.* cluster construction and heating). The large scatter observed in metal abundance and gas fraction (e.g., Davis et al. 1999) may be a reflection of this diversity.

5. Summary and Conclusions

In this paper I have attempted to construct a simple framework for understanding the relationship between the baryonic and non-baryonic components in galaxy clusters as manifest in the observed scaling of total mass, and ICM mass and central entropy with ICM temperature T_x .

Observed, as well as simulated, ICM density distributions of the most massive clusters are well-characterized by nearly isothermal hydrostatic configurations, with $f_{\text{virial}} = 0.155h_{70}^{-3/2}$ and $T_x = 1.1T_{\text{virial}}$, in an NFW potential. However, there are clear and systematic departures from the expectations derived from simply extending application of these baseline models to cooler, less massive systems. These departures are in the sense that the ICM in less massive systems have an increasingly large excess of thermal energy (from the steepening of the total mass-temperature relation), and become increasingly less concentrated – both globally (from the steepening of the total mass-temperature relation) and, more prominently, locally in the cluster core (from the flattening of the central entropy-temperature relation).

This implies that substantial heating has occurred, heating with an increasingly profound effect on less massive systems. I considered transformations of the baseline models to families of new configurations that have specified amounts of additional heating at the cluster center (and possibly different gas fractions and polytropic indices), and found that mass sequences heated by a universal amount per particle can simultaneously reproduce the observed total mass-temperature, ICM mass-temperature, and central entropy-temperature trends to excellent precision. The required central heat input is substantial, > 3 keV per particle; however, the cluster-wide average value is ~ 1 keV per particle: just consistent with robust global nucleosynthetic constraints derived from rich cluster Si abundance measurements and standard supernova energies. The concentration of the required heat injection is reflected in the fact that the local (central) entropy-temperature relation shows a more extreme departure from the gravity-only prediction than the global ICM mass-temperature relation.

The 3 keV per particle of heating required at the centers of clusters is an upper limit since it is derived assuming no pre-heating. This limit is derived from static considerations without recourse to a full dynamical treatment (with its many accompanying parameters), and becomes increasingly accurate the later the epoch of heating with respect to cluster virialization. PCN argue that the heating must occur prior to the epoch of cluster assembly. However, this is based in part on an underestimate of the available energy from supernova explosions by a factor of 3-5. If the universe as a whole is pre-heated, the total mass-temperature relation implies heating the baryons to ~ 0.5 keV at $z > 3$ which is unlikely given

that few objects with that virial temperature will have collapsed and most star formation is yet to occur. Pre-heating becomes more feasible the higher the overdensity of the proto-cluster at that epoch; however, pure pre-heating models generally require a higher entropy floor than is observed in order to reproduce the luminosity-temperature relation (equivalent to the ICM mass-temperature relation successfully reproduced by the heated mass sequence presented in Section 3.2). A strong prediction of pre-heating models is that the lowest mass clusters should be isentropic, a prediction difficult to assess with presently existing data although the entropy in the ~ 1 keV group HCG 62 appears to increase with radius.

The form of the observed departures from self-similarity would seem to imply the majority of ICM heating, *i.e.* much of the massive star formation, was contemporaneous with – and perhaps caused by – the assembly of the cluster, occurring at redshifts between 10 and 1. Comparison of more detailed evolutionary models that incorporate time- and space-dependent heating spread out over this epoch with improved X-ray observations – particularly of low-mass systems – will greatly illuminate the early star formation history of galaxies and the effect this has on the surrounding environment.

I am grateful to U. Hwang for computing and providing the data points and errorbars in Figure 2, to D. Horner for providing the data points in Figures 3 and 5, and to A. Fabian, R. Mushotzky, P. Tozzi, and the anonymous referee for providing useful feedback.

REFERENCES

- Arnaud, M., & Evrard, A. E. 1999, MNRAS, 305, 631
- Balogh, M. L., Babul, A., & Patton, D. R. 1999, MNRAS, in press
- Bird, C. M., Mushotzky, R. F., & Metzler, C. A. 1995, ApJ, 453, 40
- Bower, R. 1997, MNRAS, 288, 355
- Brighenti, F., & Mathews, W. G. 1999, ApJ, 515, 542
- Broadhurst, T. & Bouwens, R. J. 1999, ApJ, submitted
- Cavaliere, A., Menci, N., & Tozzi, P. 1999, MNRAS, in press
- Cen, R. & Ostriker, J. P. 1999a, ApJ, 514, 1
- Cen, R. & Ostriker, J. P. 1999b, ApJ, in press
- Davis, D. S., Mulchaey, J. S., & Mushotzky, R. F. 1999, ApJ, 511, 34
- Eke, V. R., Navarro, J. F., & Frenk, C. S. 1998, ApJ, 503, 569
- Ettori, S., & Fabian, A. C. 1997, MNRAS, 292, L33
- Ettori, S., & Fabian, A. C. 1999, MNRAS, in press (EF)
- Ezawa, H., Fukazawa, Y., Makishima, K., Ohashi, T., Takahara, F., Xu, H., & Yamasaki, N. Y. 1997, ApJ, 490, L33
- Finoguenov, A., & Ponman, T. J. 1999, MNRAS, 305, 325
- Fukazawa, Y. 1997, Ph.D. Thesis, University of Tokyo
- Fukazawa, Y., Makishima, K., Tamura, T., Ezawa, H., Xu, H., Ikebe, Y., Kikuchi, K., & Ohashi, T. 1998, PASJ, 50, 187
- Gibson, B. K., Loewenstein, M., & Mushotzky, R. F. 1997, MNRAS, 290, 623
- Girardi, M., Giuricin, G., Mardirossian, F., Mezzetti, M., & Boschin, W. 1998, ApJ, 505, 74
- Governato, F., Babul, A., Quinn, T., Tozzi, P., Baugh, C. M., Katz, N., & Lake, G. 1999, MNRAS, submitted
- Horner, D. J., Mushotzky, R. F., & Scharf, C. A. 1999, ApJ, in press

- Hwang, U., Mushotzky, R. F., Burns, J. O., Fukazawa, Y., & White, R. A. 1999, *ApJ*, 516, 604
- Irwin, J. A., Bregman, J. N., & Evrard, A. E. 1999, *ApJ*, in press
- Jing, Y. P. 1999, *ApJ*, submitted
- Jones, L. R., Scharf, C., Ebeling, H., Perlman, E., Wegner, G., Malkan, M., & Horner, D. 1998, *ApJ*, 495, 100
- Kay, S. T., & Bower, R. G. 1999, *MNRAS*, in press
- Kikuchi, K., Furusho, T., Ezawa, H., Yamasaki, N. Y., Ohashi, T., Fukazawa, Y., & Ikebe, Y. 1999, *PASJ*, in press
- Leitherer, C., & Heckman, T. M. 1995, *ApJS*, 95, 9
- Loewenstein, M., & Mushotzky, R. F. 1996, *ApJ*, 466, 695
- Makino, N., Sasaki, S., & Suto 1998, *ApJ*, 497, 555
- Markevitch, M. 1998, *ApJ*, 504, 27
- Markevitch, M., Forman, W. R., Sarazin, C. L., & Vikhlinin, A. 1998, *ApJ*, 503, 77
- Mathews, W. G., & Brighenti, F. 1998, *ApJ*, 503, 15
- Mohr, J. J., Mathiesen, B., & Evrard, A. E. 1999, *ApJ*, 517, 627
- Mulchaey, J. S., Davis, D. S., Mushotzky, R. F., & Burstein, D. 1996, *ApJ*, 456, 80
- Mulchaey, J. S., & Zabludoff, A. I. 1998, *ApJ*, 496, 73
- Mushotzky, R. F., & Loewenstein, M. 1997, *ApJ*, 481, 63
- Navarro, J. F., Frenk, C. S., & White, S. D. 1997, *ApJ*, 490, 493 (NFW)
- Pettini, M. 1999, in “Chemical Evolution from Zero to High Redshift,” ed. J. Walsh & M. Rosa (Berlin: Springer), in press
- Ponman, T. J., & Bertram, D. 1993, *Nature*, 363, 51
- Ponman, T. J., Cannon, D. B., & Navarro, J. F. 1999, *Nature*, 397, 135 (PCN)
- Suto, Y., Sasaki, S., & Makino, N. 1998, *ApJ*, 509, 544

Takizawa, M. 1998, ApJ, 509, 579

Timmes, F. X., Woosley, S. E., & Weaver, T. A. 1996, ApJ, 457, 834

Tozzi, P. & Norman, C. 1999, preprint

Tozzi, P., Scharf, C., & Norman, C. 1999, ApJ, submitted

White, R. E., III 1991, ApJ, 367, 69

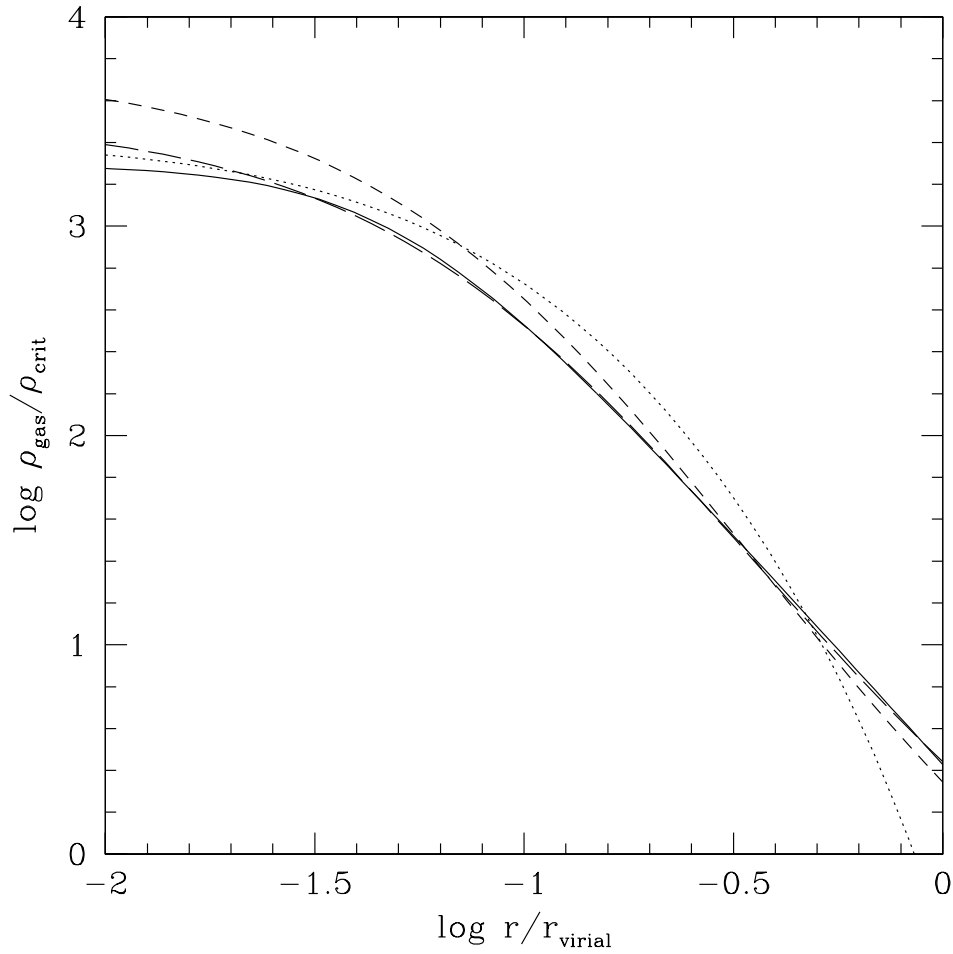


Fig. 1.— Comparison of the density profile in the following hydrostatic polytropic models with simulated cluster β -model fit (solid curve): $n = 5$ and $\tau = 1.1$ (dotted curve), $n = 100$ and $\tau = 1$ (short-dashed curve), $n = 100$ and $\tau = 1.1$ (long-dashed curve), where n is the polytropic index and τ the ratio of the emission-measure-weighted average temperature to virial temperature.

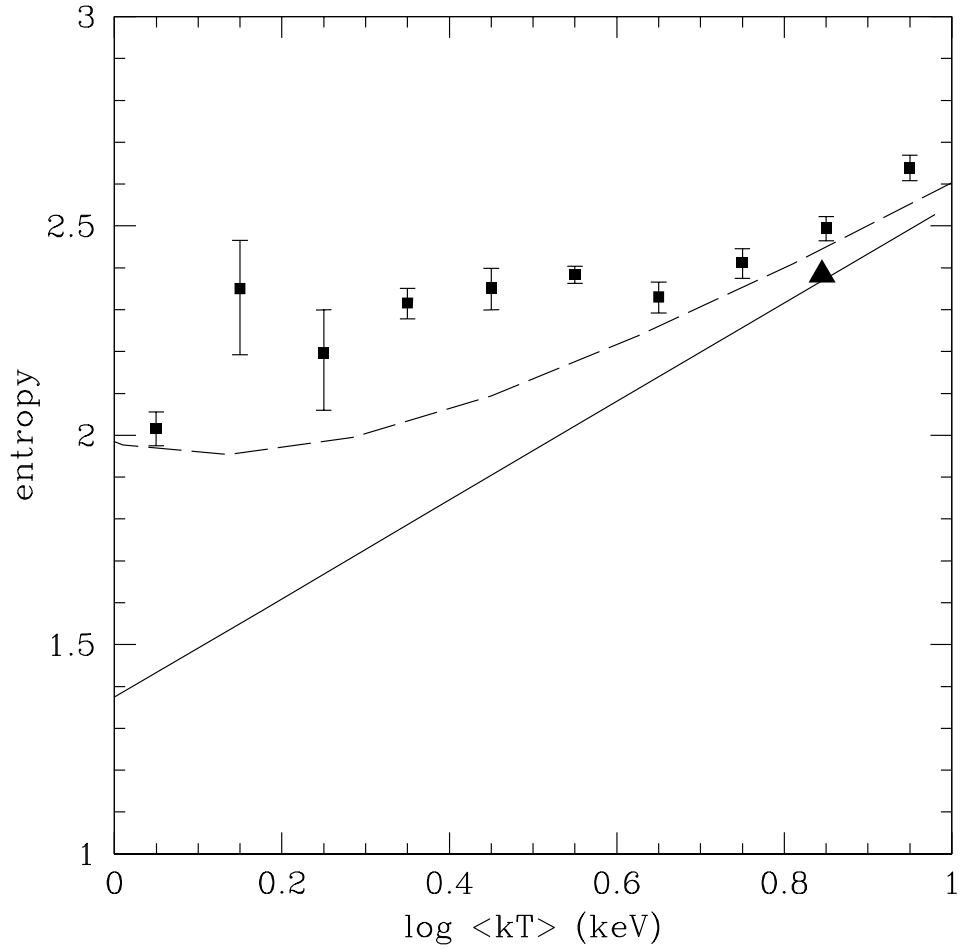


Fig. 2.— Entropy-temperature curves for heated models with $n = 100$, constant f_{virial} , and $\epsilon = 0$ (solid curve) or $\epsilon = 0.35$ (dashed curve), where the entropy is defined as $\log_{10}(kT_x n_e^{-2/3})$, n_e is in cm^{-3} and evaluated at r_c , kT_x is the average (within r_{500}) ICM temperature in keV, and $h_{70} = 1$. The filled triangle represents the value from numerical simulations without heating; the data points, representing averages in ten temperature bins, and errorbars, representing the dispersion within each bin, have been derived from *ASCA* data and kindly provided by U. Hwang.

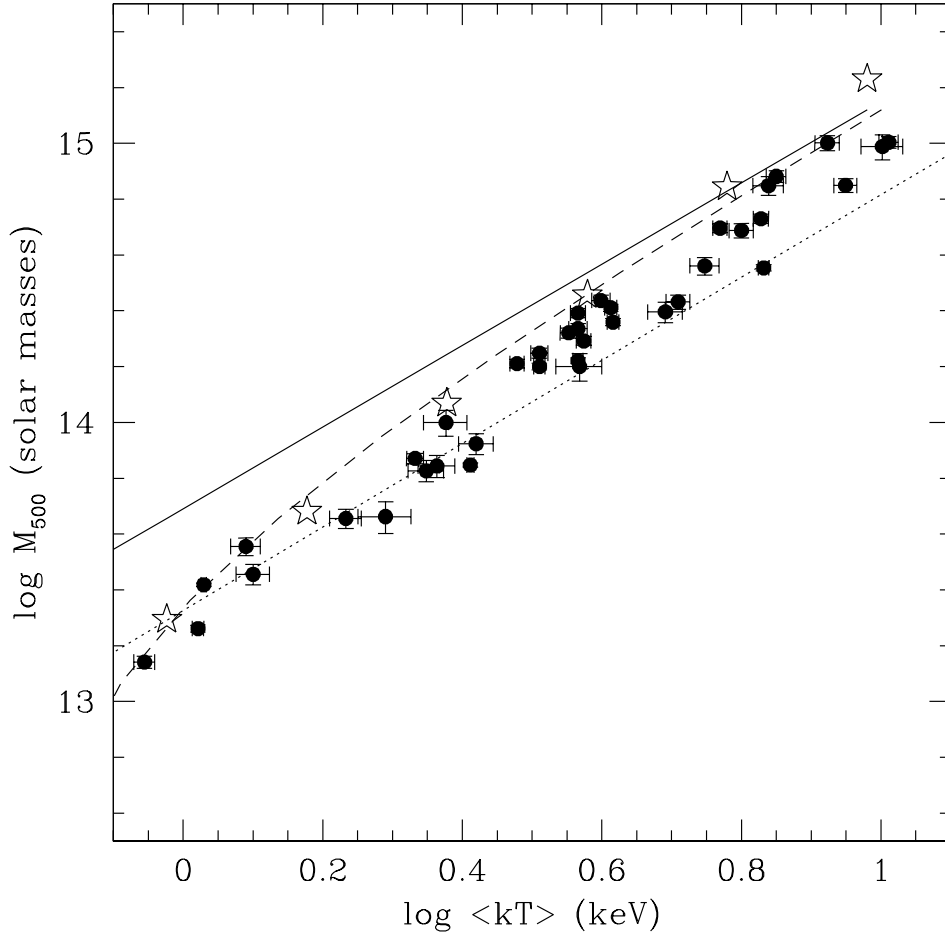


Fig. 3.— Mass-temperature curves for $\epsilon = 0$ and $\epsilon = 0.35$ models as in Figure 2, best-fit observed correlation from EF (stars), and isothermal β -model masses from Horner et al. (1999; data points with errorbars), where the mass is the total gravitational mass integrated out to r_{500} . Also shown is an isentropic mass sequence with mass-averaged temperature approximately equal to the virial temperature and $kT_x n_e^{-2/3} = 200 \text{ keV cm}^2$ (dotted curve; see Section 4.3).

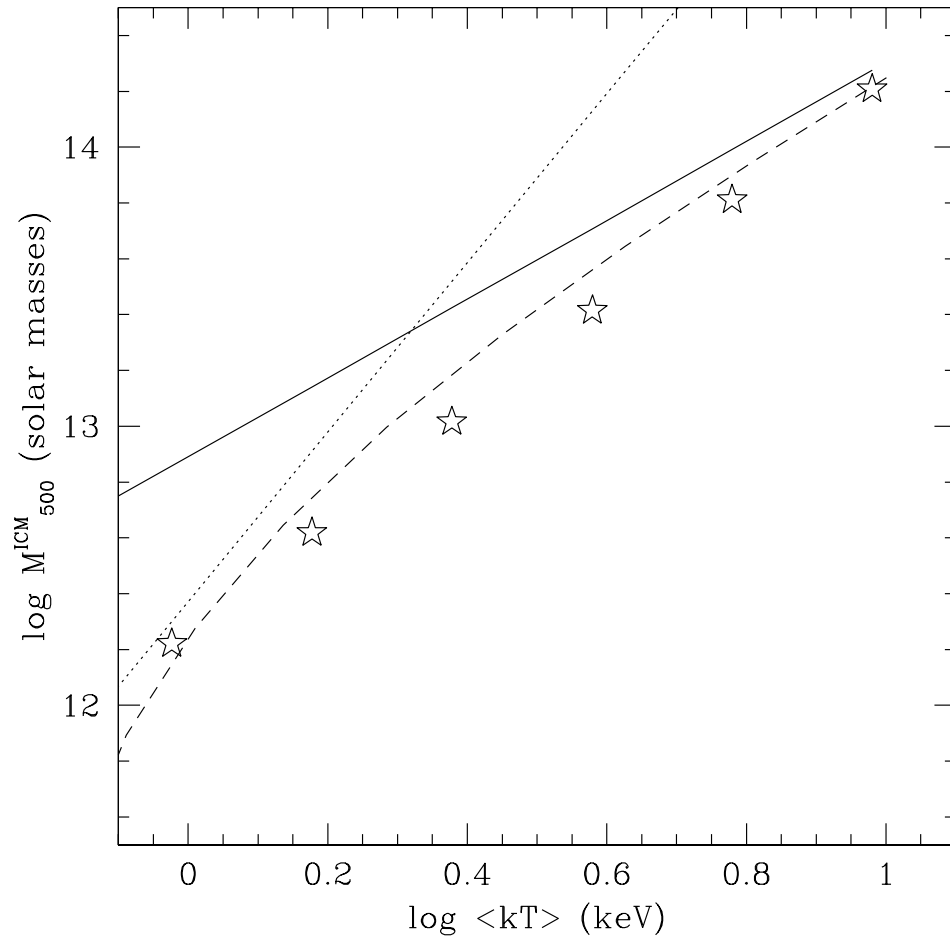


Fig. 4.— Same as Figure 3 for the ICM mass; best-fit observed correlation is from Mohr et al. (1999).

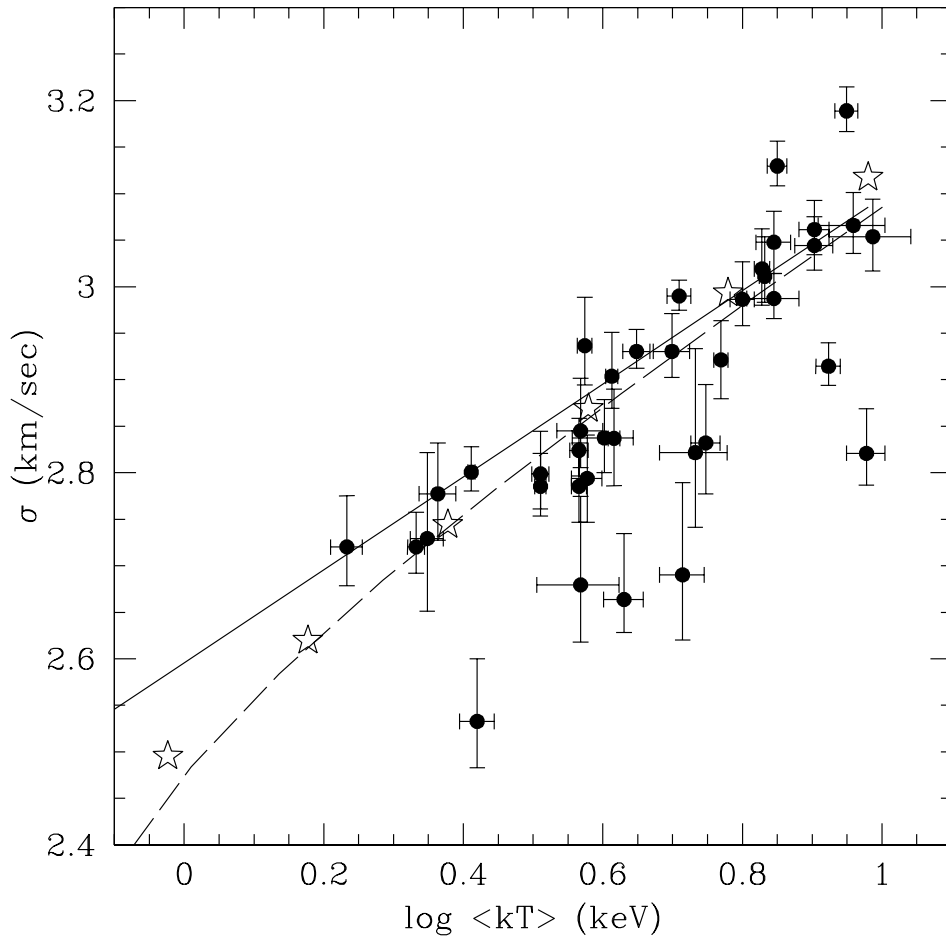


Fig. 5.— Same as Figure 3 for $(kT_{\text{virial}}/\mu m_p)^{1/2}$; observed trend is best-fit σ - T_x correlation from Bird et al. (1995); data points with errorbars are from Girardi et al. (1998).

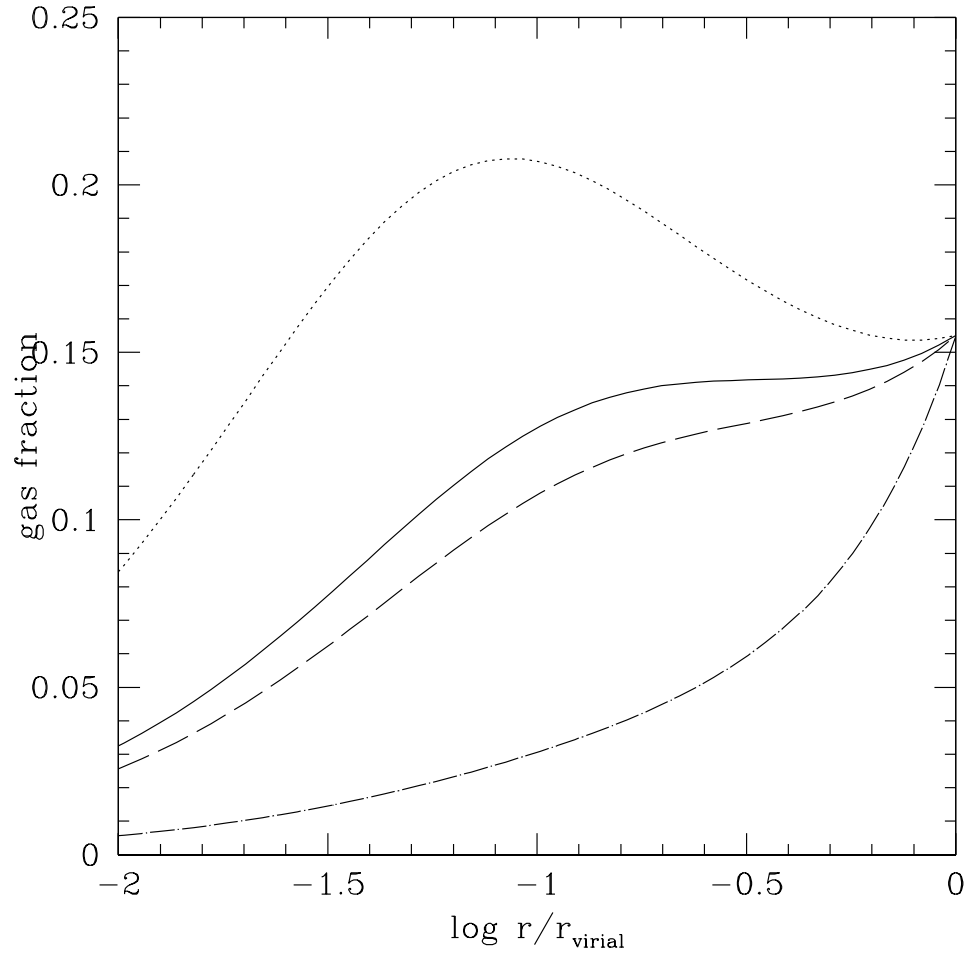


Fig. 6.— Gas fraction profiles for heated models with $n = 100$, constant f_{virial} , and $\epsilon = 0$ (solid curve: 10 keV cluster, dotted curve: 1 keV cluster) or $\epsilon = 0.35$ (dashed curve: 10 keV cluster, dot-dashed curve: 1 keV cluster).

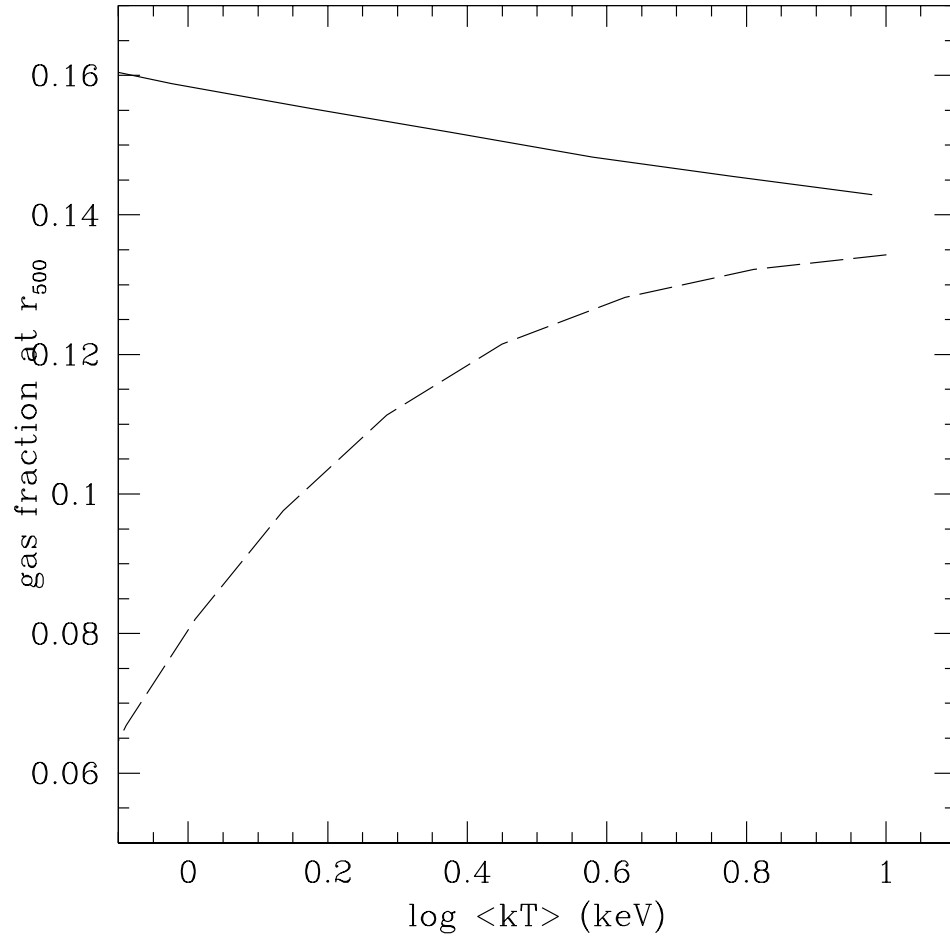


Fig. 7.— Gas fraction at r_{500} for heated models with $n = 100$, constant f_{virial} , and $\epsilon = 0$ (solid curve) or $\epsilon = 0.35$ (dashed curve).

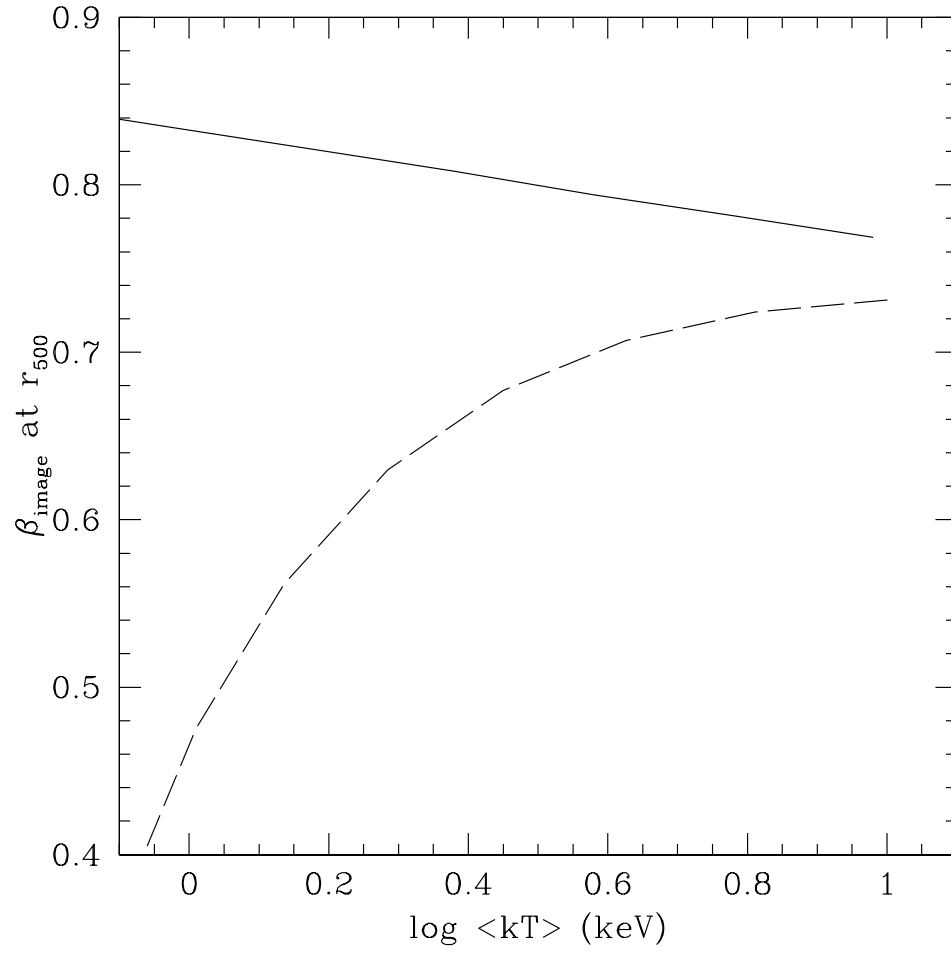


Fig. 8.— Same as Figure 7 for β_{image} (three times the ICM density slope) at r_{500} .

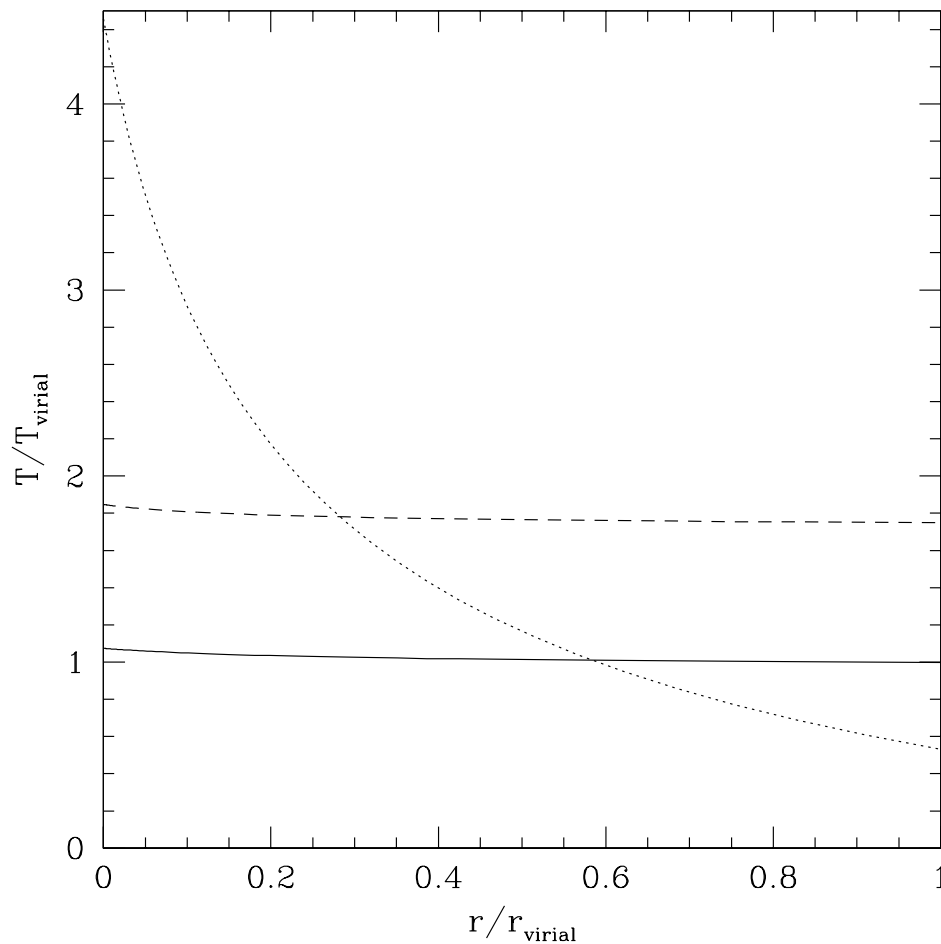


Fig. 9.— $M_{\text{virial}} = 2.3 \cdot 10^{13} M_{\odot}$ ($T_{\text{virial}} \approx 0.57$ keV) cluster temperature profiles for $\epsilon = 0$ (solid curve) and $\epsilon = 0.35$ (dashed curve) heated models featured in Figures 2-8, as well for the $kT_x n_e^{-2/3} = 200$ keV cm² isotropic model (dotted curve). The latter two models have emission-averaged temperatures ≈ 1 keV, although the mass-averaged temperature in the isotropic model is, by construction, equal to $1.05 T_{\text{virial}}$.